HETEROCYCLES, Vol. 106, No. 8, 2023, pp. 1355 - 1371. © 2023 The Japan Institute of Heterocyclic Chemistry
Received, 20th June, 2023, Accepted, 5th July, 2023, Published online, 12th July, 2023
DOI: 10.3987/COM-23-14878

SYNTHESIS, CHARACTERIZATION, AND COMPUTATIONAL STUDIES OF SOME PERFLUORINATED CYCLOPENTAPYRIDAZINES FOR BIOLOGICAL APPLICATIONS

Nathan C. Tice,[1]* Steven Wild,[1] Hannah Dendinger,[1] Bangbo Yan,[2] and Pauline Norris[2]

1. Department of Physical Sciences, University of Findlay, 1000 N. Main Street, Findlay, Ohio, 45840, USA
2. Department of Chemistry, Western Kentucky University, 1906 College Heights Blvd. Bowling Green, KY 42101, USA

*Correspondence email: tice@findlay.edu

Abstract – Fluorinated heterocycles are a major component of the field of modern medicinal chemistry due to the widespread presence of heterocyclic ring structures in naturally occurring biological molecules. The effect of the presence of fluorinated heterocyclic moieties on chemical properties such as intermolecular interactions and solubility can be used to impart synthetic molecules with useful, drug-like characteristics. Pyridazines, which are aromatic six-membered rings with a chemical formula $(CH)_4N_2$ and adjacent nitrogens, afford important biological activities to drug molecules by increasing their solubility and ability to complex with target molecules. Our method of synthesizing fluorinated pyridazines incorporates an S_NAr reaction on 5,6-fused ring pyridazines with a variety of aryl substituents at the 1- and 4-positions with pentafluoropyridine. The target products were identified by spectroscopic characterization and confirmed via X-ray crystallography. Computational studies were also performed on the phenyl-substituted case, including the calculation of an optimized structure using PBE with a cc-pVTZ basis. This analysis found the addition of perfluorinated pyridine significantly altered the esp mapping, HOMO-LUMO, and NBOs of the modified pyridazine compared to other 5,6-fused ring heterocycles.

INTRODUCTION

Fluorine's role in the design and development of pharmaceuticals continues to expand as research reveals its distinctive properties. For example, it is estimated that approximately one third of top-performing drugs on the market contain fluorine.[1] Incorporation of fluorine or fluorine containing substituents to organic compounds dramatically effects chemical activity due to the size, electronegativity, and electrostatic interactions of this unique element. Due to the strength of a carbon-fluorine bond (bond dissociation energy of 518 kJ/mol),[2] fluorine is also often introduced to improve drug stability within the body by blocking undesired chemical transformations. Physicochemical properties can also be regulated with the addition of fluorine, including basicity, which can strongly influence bioavailability and binding affinity, and lipophilicity, which allows the drug to travel more efficiently through the body.[3] Among some of the more notable fluorine containing drugs include atorvastatin (Lipitor), used to treat high cholesterol, and fluticasone propionate (Flonase), a steroidal anti-inflammatory drug.

While a variety of organic substrates can be fluorinated, heterocyclic compounds are notably susceptible to fluorine substitution.[4-7] Thus, they are common targets for enhancing biological activity via the incorporation of a fluorinated moiety, particularly with a fluorinated aromatic ring. The nucleophilic aromatic substitution (S_NAr) reaction of perfluorinated aromatics is often employed to synthesize fluorinated heterocyclic compounds because these reactions afford predictable products under mild conditions.[8,9] For example, Bhambra and coworkers isolated a series of fluoroaryl benzimidazoles via this S_NAr strategy, affording novel perfluorinated heterocycles in high yield with promising cancer inhibition properties.[8]

While pyridazines, which are six-membered aromatic rings with two adjacent nitrogens (Figure 1), have long been of interest in materials applications,[10-13] they also possess promising medicinal applications.[14-19] In general, pyridazines possess a large dipole moment with hydrogen bond acceptor sites, which leads to high solubility in water. This allows for excretion of pyridazine-derived drugs from the body after use. Specific examples of pyridazines with favorable biological activity include imidazo[1,2-*b*]pyridazines, which serve as both antimicrobial and anticancer agents.[20]

Figure 1. Pyridazine (left) and 2*H*-cyclopenta[*d*]pyridazine (right)

Given the wide variety of effective fluorine-containing pharmaceuticals available and the large number of biologically active pyridazines reported, our work focused upon the development of a series of target heterocycles which blend the unique properties of pyridazines and fluorinated aromatics. Herein, we describe and synthesis, characterization, and computational studies of some novel 5,6-fused ring pyridazines substituted with a perfluorinated pyridine ring.

RESULTS AND DISCUSSION

Synthesis and Characterization

Four newly reported perfluorinated cyclopenta[*d*][1,2]pyridazines were formed utilizing 1,2-diacylcyclopentadienes (fulvenes) reported by Linn and Sharkey.[21] In a 3 to 2 ratio, lithium cyclopentadienide was reacted with the corresponding acid chloride to afford the fulvene precursor. Formation of the previously reported 1,4-disubstituted pyridazines was accomplished utilizing the methodology by Snyder and co-workers, which was a modified procedure of Linn and Sharkey.[12,21,22] Ring closure was accomplished by reacting the fulvenes in excess hydrazine hydrate at room temperature for 24 hours (Scheme 1, Compounds **1**-**4**).

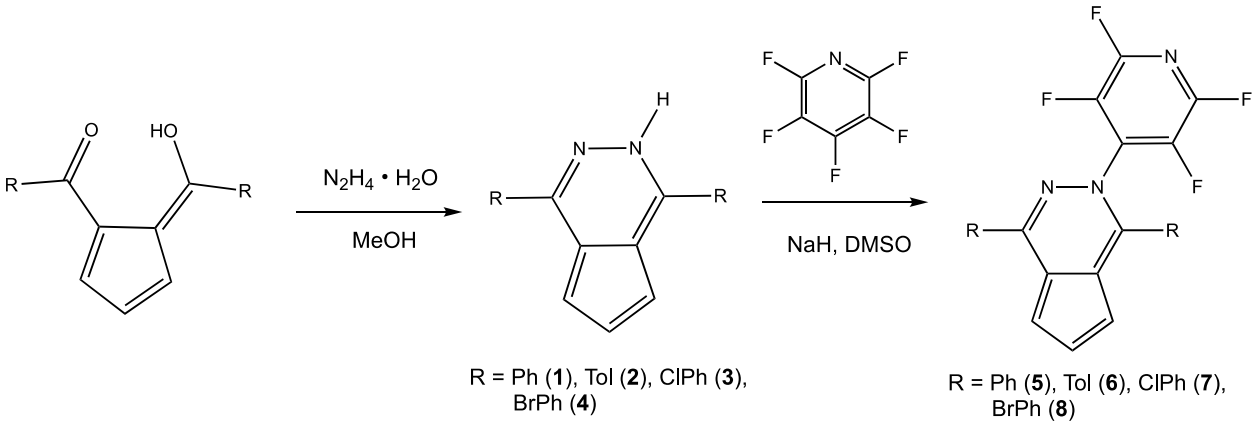

Scheme 1. Formation of perfluroinated 1,4-disubstituted cyclopentapyridazines

The 5,6-fused ring pyridazines were then substituted with a perfluorinated pyridazine employing the modified procedure reported by Bhambra and coworkers. Reaction of the pyridazines with sodium hydride followed by pentafluoropyridazine at room temperature in DMSO afforded the desired S_NAr products in good to high yield (60-90%, compounds **5**-**8**). Isolated yields were improved with the chloro- and bromophenyl cases by mildly heating the product mixture after quenching, which allowed for more effective filtration of the product (compounds **7** and **8** were especially fine and difficult to isolate via filtration). The target fluorinated pyridazines all displayed high stability in air and organic solvents.

^{1}H NMR spectroscopy confirms the structures for the fluorinated pyridazines **5**-**8**, showing both

asymmetric Cp and aryl substituents. The range of chemical shifts (6.8-8.0 ppm) is typical for fused-ring Cp protons.[23-25] For certain cases, like compound **5**, one of the unique Cp signals could not be resolved from those attributed to the aryl substituents. However, other spectra, including compound **6**, clearly shows the 3 separate Cp signals in this range. To demonstrate complete conversion on the pyridazine starting materials **1-4**, we did not observe any trace of the characteristic N-H resonances in the 11-13 ppm range. Also observed in the ^{13}C NMR spectroscopy were the complex Cp and aryl ring signals (from 112 to 151 ppm) due to the addition of the fluorinated ring as well as the asymmetric nature of the target products. Characterization via IR spectroscopy of compounds **5-8** also showed the disappearance of the stretch at 3200 cm^{-1}, characteristic of an N-H stretch. The IR spectra for each fluorinated pyridazine also displayed a set of newly formed C=N stretches at approximately a 1580 cm^{-1}. High resolution mass spectrometry also confirms the molecular structures of compounds **5-8**, with the expected $M^+ + 1$ ion peak observed for each case. Mass accuracies for each compound were 1.3 ppm or less compared to calculated values. Elemental analysis was performed for the new fluorinated pyridazines **5-8**, which confirmed the desired molecular formula and analytical purity for each case. Experimental details and characterization for compounds **5-8** are given in the Experimental section.

X-Ray Crystallographic Analysis

The structure of the phenylpyridazine **5** was further confirmed by single-crystal X-ray diffraction methods (Figure 2). Suitable crystals for analysis were grown by slow evaporation from a methylene chloride solution at ambient temperature and isolated as orange-red plates. Compound **5** crystallized with a monoclinic lattice (space group P2/c), with two independent molecules in the asymmetric unit, and thus there are 8 molecules total in the unit cell.

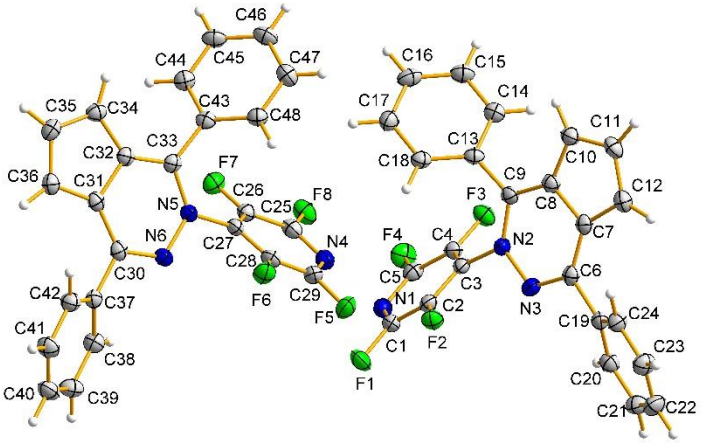

Figure 2. ORTEP stereographic projections of molecules A (left) and B (right) of the structure of phenyl-pyridazine **5** at 150 K. Thermal ellipsoids are plotted at the 50% probability level.

X-Ray crystallographic analysis reveals that the central cyclopentadienyl pyridazine ring for both molecules A and B are highly planar, with the root mean square deviation of the fitted atoms at 0.0229 and 0.0185 respectively. By contrast, both the aryl rings and the fluorinated pyridazyl ring for each unique molecule are highly tilted out of the plane created by the central 5,6-fused ring. The planes incorporating the aryl carbons C13-C18, C19-C24, and C1-N1 in molecule A have a torsional angle of 50.19°, 40.62°, and 54.85° to the central ring respectively. The analogous torsional angles for molecule B are 42.78° (C37-C42), 49.10° (C43-C48), and 54.91° (C25-N4). This highly twisted conformation of the side aryl rings is typical of 5,6-fused pyridazines.[12,22] Tables of crystallographic details, atomic coordinates and displacement parameters, bond distances and angles, intermolecular contact distances, structure factors and a crystallographic information file (CIF) for the structure of **5** have been deposited with the Cambridge Crystallographic Data Centre.[26]

Computational Studies

Conformational analysis

All computations were performed involving the phenylpyridazine **5** using the Gaussian 16 program,[27] and Gauss-View 6 molecular visualization package[28] was used for processing the output. While the original crystallographic unit cell of compound **5** had 2 molecules, optimizations presented here are on the individual molecules. No noticeable differences were observed between the two systems, so other than for conformational analysis, only molecule B was chosen for the computational studies to prevent redundancy. With respect to the preferred geometry, analyzing this optimized structure for compound **5** will aid in understanding the feasibility of docking at particular sites of interest within biological systems. The optimized conformations of molecules A and B are shown in Figure 3. Geometry optimization was carried out with DFT methods in a series of steps. The beginning optimization utilized B3LYP with a 6-31G basis set, with the optimization presented here calculated using the Perdew-Burke-Ernzerhof (PBE) generalized gradient exchange-correlation functional[29] and a triple-zeta correlation consistent (cc-pVTZ) basis.[30]

The PBE functional and cc-pVTZ basis were chosen so direct comparisons could be made to previous work.[13,25] After optimization, a single point energy was found with the PBE functional with the cc-pVTZ basis to ensure the lowest energy state. No imaginary frequencies were observed in the optimized results presented. The optimized geometries were further checked by comparing the bond angles and lengths using a Pearson correlation coefficient between the two. The correlation coefficient, which is a measure of the linear correlation between two variables, was calculated by the following equation:

$$\frac{n\sum xy - \sum x \sum y}{\sqrt{n\sum x^2 - (\sum x)^2}\sqrt{n\sum y^2 - (\sum y)^2}}$$

For this correlation coefficient equation, x is the theoretical values from the crystal structures and y is the corresponding values from the optimized geometries. Typically, this affords values between -1 and +1, where -1 is a total negative linear correlation, 0 is no linear correlation and +1 indicates a positive linear correlation.[31,32] The correlation coefficient observed for bond angles and bond lengths for compound **5** were 0.98 and 0.99 respectively. These values demonstrate alignment between bond lengths and angles among the observed crystal structure and optimized structure. However, while the torsion angles are not in as good agreement with a coefficient of 0.49, differences observed are mainly due to the orientation of the xyz reference axis (Figure 4). The different orientation of the axis will lead to different measured results for the torsional angles. While some torsional differences can be seen between molecules A and B, these variations are small and do not significantly alter the lowest energy conformation between each structure. For example, the torsion angle for the crystal for C12-N5-C8-F1 is -179.61°, contrasting with the optimized structure angle of 179.54°. This large difference between negative values observed in the crystal structure and positive sign on the optimized structure occurs on 12 of the 116 torsion angles reported. These deviations observed are most likely due to optimizations performed in the gas phase, which lack the molecular interactions such as Van der Waals forces and dipole-dipole interactions.[33,34] The gas phase would also allow for free rotation, leading to the torsion angles to flip to the negative side of the measure axis. However, as shown in Figure 5, there is little discernable different in the optimized structure of either molecule.

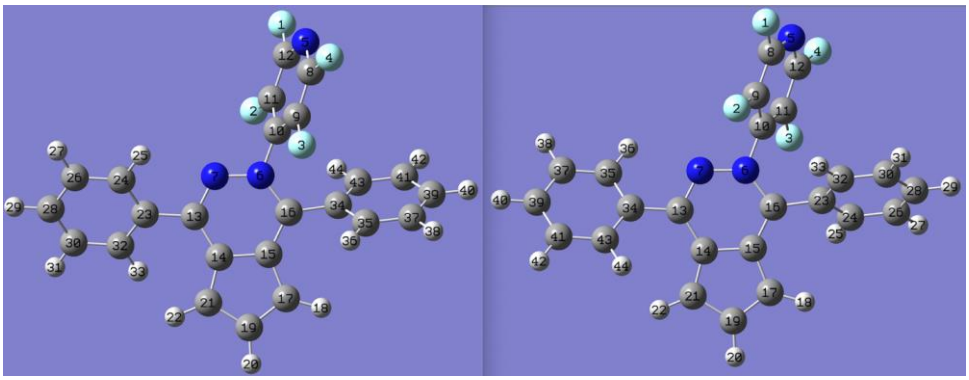

Figure 3. Optimized geometry for molecules A (left) and B (right)

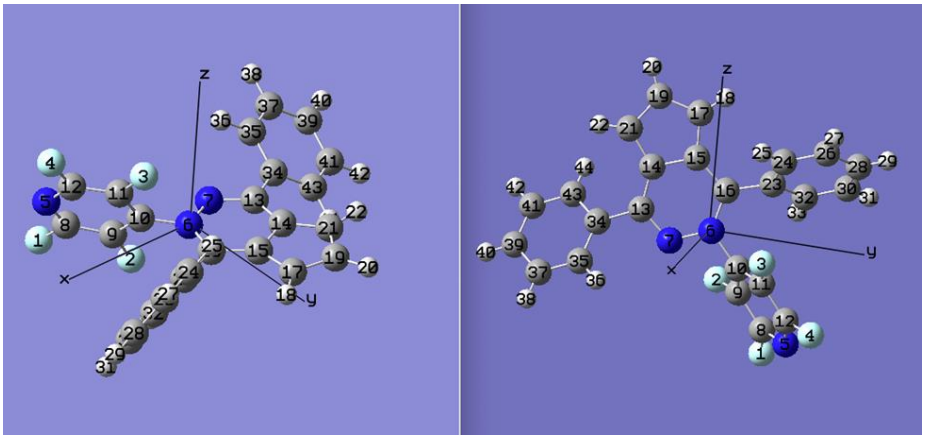

Figure 4. Observed orientation around reference axis in optimized geometry of molecule B (left) and original crystal (right)

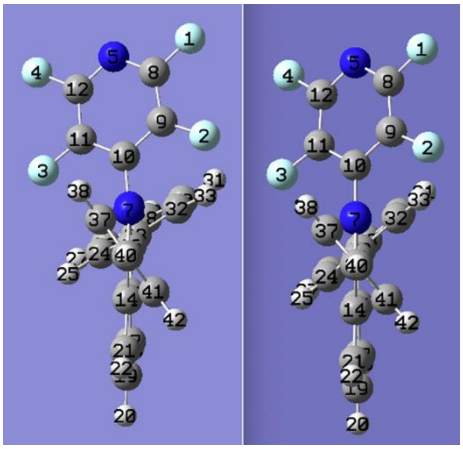

Figure 5. End on view of optimized structure of molecule B (left) and crystal B (right)

Some additional key some torsion angles of interest include those involving the aryl side chains and the central pyridazine ring. Table 1 summarizes these differences between the crystal and optimized structures, with variations observed again due to the additional constraining factors of the solid verses the gas phase.

Table 1. Observed Differences in Molecule B for Aryl Ring Torsional Angles

Torsional Angle	Crystal (°)	Optimized (°)
N7-N6-C10-C9	52.28	66.28
C10-N6-C16-C23	1.12	9.45
N7-C13-C34-C35	40.85	36.17

Electrostatic Potential Maps

To help visualize charge distributions and electronic properties, an electrostatic potential (esp) map was created for phenylpyridazine **5** using PBE functional with the cc-pVTZ basis (Figure 6). This is a single surface counter (isovalue 0.004) and has electrostatic potential between -0.05 and +0.05. The red color (-0.05 eV) shows lower electrostatic potential values (electron-rich) and blue (+0.05 eV) is a higher value (electron-poor). With respect to docking, the red regions indicate an area that would be ideal for nucleophilic (proton) binding, and the blue regions are ideal for electrophilic (electron) binding. When analyzing the esp mapping both molecules A and B, both the nitrogen within the pyridine ring (N5) and the nitrogen in the central pyridazine ring (N7) show regions of high electron density, indicating potential favorable proton binding. By contrast, the hydrogens on the phenyl rings and the carbons with the pyridine ring are highly electron deficient, which indicates regions ideal for electron binding. These areas of both high and low electron density should enhance the binding affinity within the cell. When compared to non-fluorinated cases studied previously,[12,13,22,23] some similarities and differences are noted. The N7 nitrogen atom is slightly electron rich, which is observed in prior studies. However, based on the size and intensity of the red region on the esp mapping, this nitrogen is not as electron rich as previously reported 5,6-fused Cp heterocycles. The electron mapping on the Cp ring is similar to those of other fused-pyridazines with and exception of the those reported with thienyl side groups.[13,25] Cp rings on thienyl-containing pyridazines were observed to be more electron rich. Another notable difference is that previously reported pyridazines lack the fluorinated ring on bound to a nitrogen (N6). Those nitrogen positions are relatively electron poor and serve as good sites for electron binding. With the addition of the fluorinated pyridine, an electron rich site (N5) has been introduced at that same position.

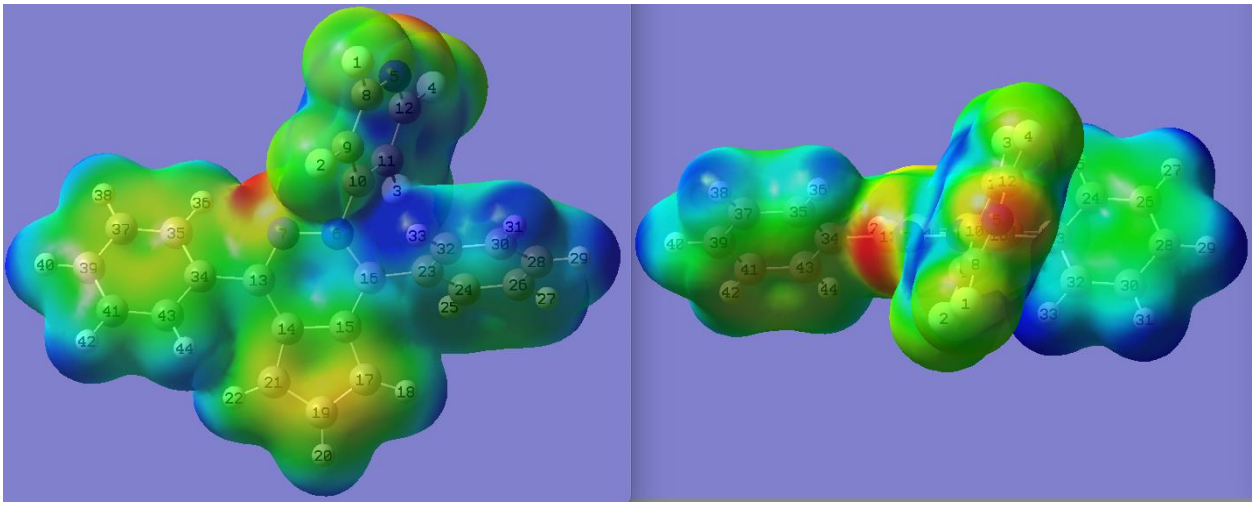

Figure 6. Esp mapping for Molecule B showing the pyridazine face (left) and a top-down perspective. Red regions show areas of electron rich centers and blue areas are ideal for electron binding.

HOMO-LUMO Analysis

The HOMO-LUMO data shown was calculated on molecule B using the Perdew-Burke-Ernzerhof (PBE) generalized gradient exchange-correlation functional[29] and a triple-zeta correlation consistent (cc-pVTZ)[30] basis with canonical molecular orbitals (Figure 7). The calculated HOMO for pyridazine **5** occupies space completely on the central ring. By contrast, the LUMO is more dispersed throughout the molecule, with significant portions on the central pyridazine, one of the phenyl moieties (containing C34), and the pyridine ring. As a large portion of the LUMO is observed within the fluorinated ring, this analysis indicates that the addition of the pyridine ring should modify the electronic properties of this series of pyridazines and potentially lead to differences in biological activity as compared to their unsubstituted precursors.

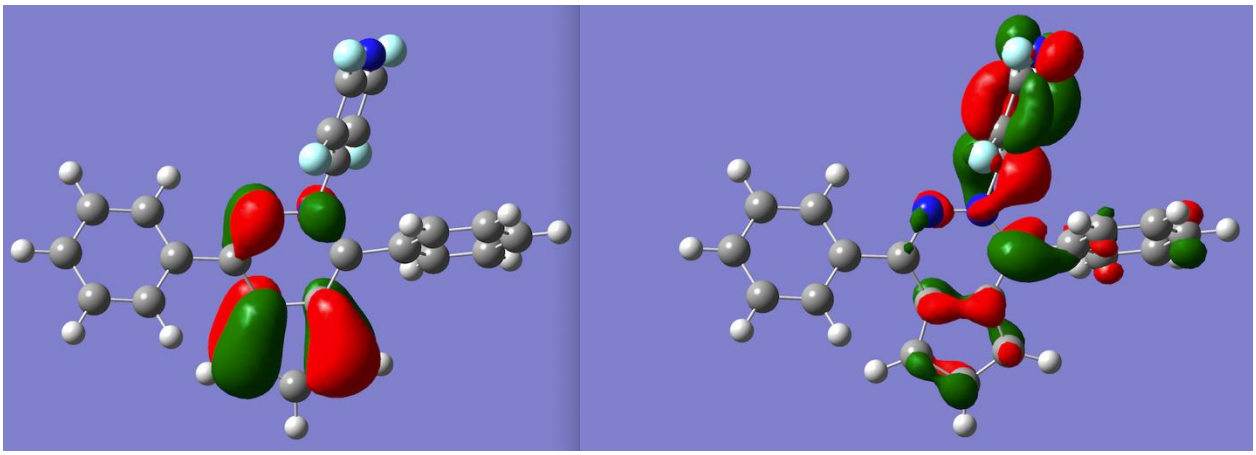

Figure 7. The calculated HOMO -0.18359 ev (left) and LUMO -0.10428 ev (right)

Natural Bond Analysis

A Natural Bond Orbital analysis was done to help visualize and interpret electronic orbitals and further the understanding of intra- and intermolecular interactions in these systems (Figures 8 and 9). These calculations were performed with PBE-cc-pVTZ methods using NBO 3.1.[34] The second order Fock matrix was carried out to examine the donor-acceptor interactions. A larger calculated stabilization energy indicates a stronger interaction between electron donors (Lewis Type) and acceptors (anti-bonding or Rydberg). These interactions show an overall delocalization of electron density which helps with stabilization. Goekce et al. noted that while there is no direct relationship between NBO analysis and molecular docking studies, the reactive sites and highest stabilizations calculated are the basis of receptor-ligand interactions for molecular docking studies.[35] Other work by Agwupuye et al.[36] and Kumar et al.[37] also report the usefulness of the NBO studies as possible target sites for inter- and intra-molecular interactions. These observations make NBO calculations a useful guide for targeting binding locations in

biological systems.

Upon analysis of the NBOs for molecule B, there are several donor-acceptor pairs of interest. The first involves the lone-pair electrons on the nitrogen within the pyridazine ring (N6) (Figure 8). These electrons interact with the neighboring antibonding carbon-carbon bond (C15-C16) and nitrogen-carbon bond (N7-C13), with stabilization energy values of 31.83 and 21.66 kcal/mol respectively. These stabilization values indicates large delocalization in molecule B. This type of strong delocalization has been observed in the central moiety of fused-ring systems, including 14.22 to 28.56 kcal/mol values reported for thienyl oxazine interactions[25] and 12.88 to 36.49 kcal/mol for pyridazine and oxazine systems.[13]

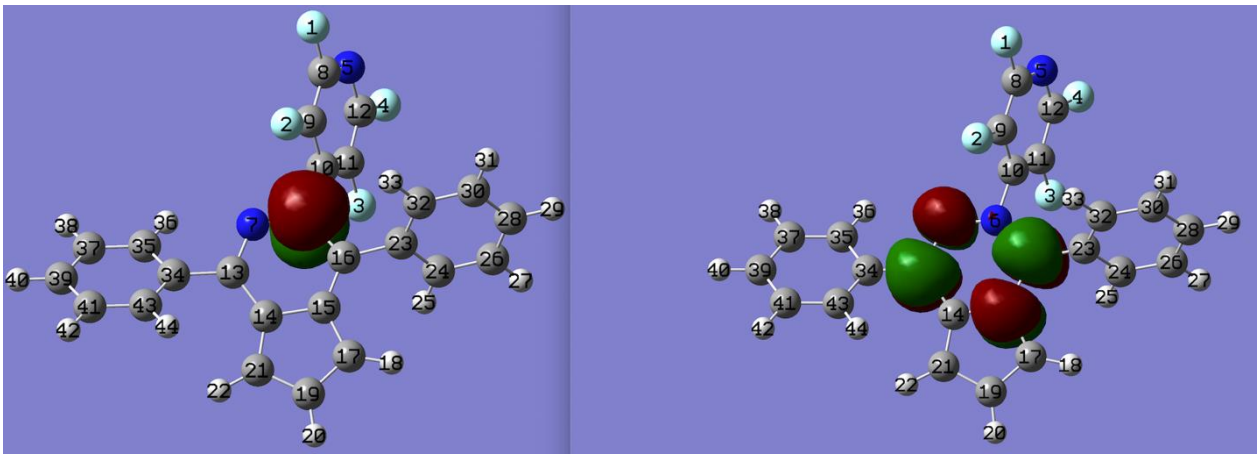

Figure 8. N6 lone-pair donor orbital and C15-C16 and N7-C13 anti-bonding acceptor orbital for molecule B

Another stabilization for this system involves the interaction of the lone pairs on the fluorine atoms with the antibonding pyridine carbon and nitrogen-carbon bonds (Figure 9). The stabilization energies observed for this interaction is slightly below those involving the central pyridazine, with values at 18.52 to 22.14 kcal/mol for molecule B. However, these still represent significant donor-acceptor interactions and demonstrate the impact that the addition of the fluorinated ring can have on the electronic properties on the pyridazine substrate.

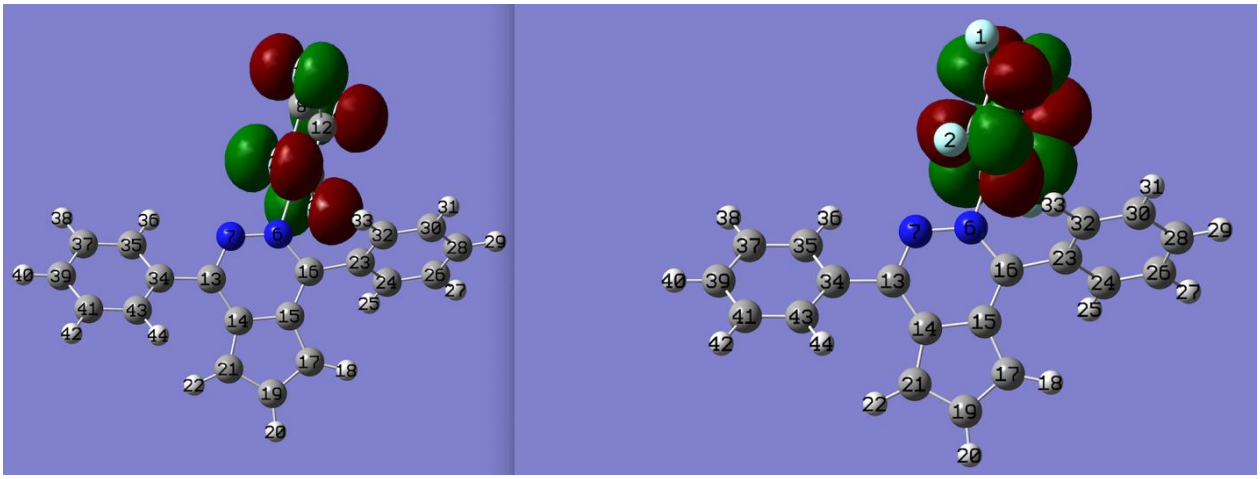

Figure 9. Fluorine atom lone pairs donating orbitals and ring atom antibonding acceptor orbitals

EXPERIMENTAL

All reactions were carried out using standard Schlenk techniques under a nitrogen atmosphere unless otherwise noted. NMR solvent chloroform-*d* (Acros), magnesium sulfate, MeOH (VWR), anhydrous DMSO, hydrazine hydrate, CH_2Cl_2, pentafluoropyridine, sodium hydride (Aldrich) were all used without further purification. The 1,2-diacylcyclopentadiene precursors were all made according to previously reported procedures.[21] ^{1}H and ^{13}C NMR spectra were recorded on a Varian 400 MHz NMR spectrometer at ca. 22 °C and were referenced to residual solvent peaks and TMS internal standard. All ^{13}C NMR spectra were listed as decoupled. All infrared spectra were recorded on a Perkin Elmer Spectrum One FT-IR Spectrometer. The mass spectrometry analysis was performed with a Synapt high-definition mass spectrometer with a nano-electrospray ionization (ESI) source and Time of Flight (TOF) as mass analyzer (Waters, Milford, MA). The experimental condition included a 60 μL/min flowrate and the capillary voltage of 3.0 V. Melting points were taken on a standard Mel-Temp apparatus.

General synthesis of 1,4-disubstituted pyridazines (**1**-**4**):

Pyridazines **1**-**4** were prepared according to literature procedures.[12,21,22] In a 100 mL Schlenk flask, 500 mg of starting appropriate 1,2-diacylcyclopentadiene was reacted with 3 mL of hydrazine hydrate in 30 mL of MeOH (Scheme 1). The reactions were kept under inert atmosphere at room temperature and stirred overnight. The solutions were quenched with water and extracted with CH_2Cl_2 (3 x 25 mL). The organic layers were collected, dried over $MgSO_4$, and filtered. The volatiles were removed *in vacuo* to afforded pyridazines **1**-**4**, which were characterized by IR and ^{1}H NMR and compared to reported values.

General experimental procedure for fluorinated pyridazines (**5**-**8**)

The synthetic methodology utilized is a modified version reported by Bhambra et al.[8] To a 100 mL Schlenk flask, excess pentafluoropyridine (1.5 equivalents) and sodium hydride (1.5 equivalents) were added to 10 mL of DMSO under inert atmosphere. Approximately 250 mg of substituted pyridazine was added at room temperature and stirred for 18 h. The reaction was quenched with water and the suspension was filtered and allowed to dry. For compounds **7** and **8**, additional product was isolated by gently boiling the filtrate for 20 min, allowing the mixture to cool, then isolating the suspended product. Analytically pure samples were prepared by dissolving the crude product in CH_2Cl_2, filtering and removing the volatiles *in vacuo*, and finally triturating with cold pentane.

*Synthesis of 2-(perfluoropyridin-4-yl)-diphenyl-2H-cyclepenta[d]pyridazine (**5**):*

Pyridazine **1** (256 mg) was reacted using the general procedure described above to form the fluorinated pyridazine **5**, as a yellow-orange solid (231 mg, 59.8%). **Mp** 145-147 °C (decomposed). **^{1}H NMR (400 MHz, $CDCl_3$, ppm):** 6.88 (dd, 1H, J_3 = 4.4 Hz, J_4 = 1.2 Hz, Cp), 7.15 (dd, 1H, J_3 = 3.2 Hz, J_4 = 1.2 Hz, Cp), 7.46-8.01 (m, 11H, Ph/Cp).**^{13}C NMR (100 MHz, $CDCl_3$, ppm):** 112.62, 113.22, 119.45, 124.07, 128.93, 128.96, 129.04, 129.15, 130.98, 131.05, 131.13, 134.83, 136.36, 146.20, 151.40. **IR (cm^{-1}):** 1586 (N=C). **HRMS:** *m/z* Calc: 420.1124. Found: 420.1122 (M^+ + 1). Anal. Calcd for $C_{24}H_{13}F_4N_3$; Calc: C, 68.74; H, 3.12; N, 10.02. Found: C, 69.11; H, 2.99; N, 10.23.

The crystal structure of **5** was determined from single-crystal X-ray diffraction intensity measurements. An orange-red crystal, typical of others in a batch grown by slow evaporation from a CH_2Cl_2 solution at room temperature, was selected for data collection. The total exposure time was 60.21 h at temperature of 150 K. Twinning domains were determined using CELLNOW.[38] The structure was integrated and refined as a two domain nonmerohedral twin with a domain ratio of 0.82:0.18. The two domains are related by a 180° rotation around the c-axis. The frames were integrated with the Bruker SAINT software package[39] using a narrow-frame algorithm. The structure was solved and refined using the Bruker SHELXTL Software Package[40] using the space group P2/c, with Z = 8 for the formula unit, $C_{24}H_{13}F_4N_3$. Data were corrected for absorption effects using the Multi-Scan method (SADABS).[41] Crystal data and a summary of experimental details are given in Table 2.

Table 2. Sample and crystal data for compound **5**

Chemical formula	$C_{24}H_{13}F_4N_3$	
Formula weight	419.37 g/mol	
Temperature	150(2) K	
Wavelength	1.54178 Å	
Crystal system	Monoclinic	
Space group	P 1 2/c 1	
Unit cell dimensions	a = 21.4720(6) Å	α = 90°

	b = 9.7059(3) Å	β = 111.901(1)°
	c = 19.6996(5) Å	γ = 90°
Volume	3809.20(19) $Å^3$	
Z	8	
Density (calculated)	1.463 g/cm^3	
Absorption coefficient	0.982 mm^{-1}	
F(000)	1712	
Theta range for data collection	2.22 to 62.43°	
Reflections collected	10538	
Coverage of independent reflections	97.9%	
Absorption correction	Multi-Scan	
Structure solution technique	direct methods	
Structure solution program	XT, VERSION 2018/2	
Refinement method	Full-matrix least-squares on F2	
Refinement program	SHELXL-2018/3 (Sheldrick, 2018)	
Function minimized	Σ w(Fo2 - Fc2)2	
Data / restraints / parameters	10538 / 0 / 560	
Goodness-of-fit on F2	1.053	
Final R indices	9457 data; I>2σ(I)	R1 = 0.0305, wR2 = 0.0780
	all data	R1 = 0.0354, wR2 = 0.0843
Weighting scheme	$w=1/[\sigma^2(F_o^2)+(0.0432P)^2+0.7199P]$ where $P=(F_o^2+2F_c^2)/3$	
Largest diff. peak and hole	0.173 and -0.191 $eÅ^{-3}$	
R.M.S. deviation from mean	0.035 $eÅ^{-3}$	

*Synthesis of 2-(perfluoropyridin-4-yl)-1,4-di-p-tolyl-2H-cyclopenta[d]pyridazine (**6**)*

Pyridazine **2** (253 mg) was reacted using the general procedure described above to form the fluorinated pyridazine **6**, as a yellow-orange solid (231 mg, 61.7%). **Mp** 155-157 °C. **^{1}H NMR (400 MHz, $CDCl_3$, ppm):**

2.42 (s, 3H, Me), 2.45 (s, 3H, Me), 6.87 (d, 1H, J_3 = 4.4 Hz, Cp), 7.13 (d, 1H, J_3 = 2.8 Hz, Cp), 7.49 (t, 1H, J_3 = 4.4 Hz, Cp) 7.24 (d, 2H, J_3 = 7.6 Hz, Ph), 7.35 (d, 2H, J_3 = 7.6 Hz, Ph), 7.39 (d, 2H, J_3 = 8 Hz, Ph), 7.89, 7.24 (d, 2H, J_3 = 8 Hz, Ph). **^{13}C NMR (100 MHz, $CDCl_3$, ppm):** 21.44, 21.50, 112.19, 112.88, 119.20, 123.77, 127.91, 128.62, 128.84, 129.39, 129.54, 133.37, 134.19, 139.82, 141.23, 146.24, 151.14. **IR (cm^{-1}):** 1580 (N=C). **HRMS:** *m/z* Calc: 448.1436. Found: 448.1433 (M^+ + 1). Anal. Calcd for $C_{26}H_{17}F_4N_3$; C, 69.79; H, 3.83; N, 9.39. Found: C, 70.18; H, 3.80; N, 9.44.

*Synthesis of 2-(perfluoropyridin-4-yl)-1,4-dichlorophenyl-2H-cyclopenta[d]pyridazine (**7**):*

Pyridazine **3** (253 mg) was reacted using the general procedure described above to form the fluorinated pyridazine **7**, as a yellow-orange solid (266 mg, 74.1%). **Mp** 162-164 °C (decomposed). **^{1}H NMR (400 MHz, $CDCl_3$, ppm):** 6.85 (d, 1H, J_3 = 4.4 Hz, Cp), 7.13 (d, 1H, J_3 = 3.2 Hz, J_3 = 2.8 Hz, Cp), 7.46-7.96 (m, 9H, Ph/Cp). **^{13}C NMR (100 MHz, $CDCl_3$, ppm):** 112.58, 113.08, 118.92, 124.07, 129.01, 129.11, 129.39, 130.04, 130.24, 134.45, 135.26, 135.98, 137.49, 144.71, 150.03. **IR (cm^{-1}):** 1588 (N=C). **HRMS:** *m/z* Calc: 488.0344. Found: 488.0346 (M^+ + 1). Anal. Calcd for $C_{24}H_{11}Cl_2F_4N_3$; C, 59.04; H, 2.27; N, 8.61. Found: C, 58.96; H, 2.31; N, 8.44.

*Synthesis of 2-(perfluoropyridin-4-yl)-1,4-dibromophenyl-2H-cyclopenta[d]pyridazine (**8**):*

Pyridazine **4** (250 mg) was reacted using the general procedure described above to form the fluorinated pyridazine **8**, as a yellow-orange solid (301 mg, 90.4%). **Mp** 152-154 °C. **^{1}H NMR (400 MHz, $CDCl_3$, ppm):** 6.85 (dd, 1H, J_3 = 4.4 Hz, J_4 = 1.2 Hz, Cp), 7.12 (dd, 1H, J_3 = 3.2 Hz, J_4 = 0.8 Hz, Cp), 7.38 (d, 2H, J_3 = 8.4 Hz, Ph), 7.45 (dd, 1H, J_3 = 3.2 Hz, J_3 = 3.2 Hz, Cp), 7.62 (d, 2H, J_3 = 8.4 Hz, Ph), 7.68 (d, 2H, J_3 = 8.8 Hz, Ph), 7.88 (d, 2H, J_3 = 8.4 Hz, Ph). **^{13}C NMR (100 MHz, $CDCl_3$, ppm):** 112.61, 113.11, 118.83, 124.02, 124.30, 125.84, 129.58, 130.28, 130.40, 131.97, 132.34, 134.91, 135.30, 144.73, 150.08. **IR (cm^{-1}):** 1588 (N=C). **HRMS:** *m/z* Calc: 575.9334. Found: 575.9326 (M^+ + 1). Anal. Calcd for $C_{24}H_{11}Br_2F_4N_3$; C, 49.94; H, 1.92; N, 7.28. Found: C, 50.32; H, 1.97; N, 7.30.

ACKNOWLEDGEMENTS

We wish to thank our sources of support for this research, including the Department of Physical Sciences and the Faculty Development Committee at the University of Findlay

REFERENCES AND NOTES

1. J. Wang, M. Sánchez-Roselló, J. L. Aceña, C. del Pozo, A. E. Sorochinsky, S. Fustero, V. A. Soloshonok, and H. Liu, *Chem. Rev.*, 2014, **114**, 2432.
2. J. Rumble, 'CRC Handbook of Chemistry and Physics', 102nd Edition, Taylor & Francis, New York,

2021.

3. H. Böhm, D. Banner, S. Bendels, M. Kansy, B. Kuhn, K. Müller, U. Obst-Sander, and M. Stahl, *ChemBioChem*, 2004, **5**, 637.
4. T. Hiyama and M. Shimizu, *Angew. Chem. Int. Ed.*, 2005, **44**, 214.
5. G. M. Brooke, *J. Fluorine Chem.*, 1997, **86**, 1.
6. M. W. Cartwright, L. Convery, T. Kraynck, G. Sandford, D. S. Yufit, J. A. K. Howard, J. A. Christopher, and D. D. Miller, *Tetrahedron*, 2010, **66**, 519.
7. I. T. Suydam and S. A. Strobel, *J. Am. Chem. Soc.*, 2008, **130**, 13639.
8. A. Bhambra, M. Edgar, M. Elsegood, L. Horsburgh, V. Krystof, P. Lucas, M. Mojally, S. Teat, T. Warwick, G. Weaver, and F. Zeinali, *J. Fluorine Chem.*, 2016, **188**, 99.
9. R. Ranjbar-Karimi, M. Mashak-Shoshtari, S. Hashemi-Uderji, and R. Kia, *J. Fluorine Chem.*, 2011, **132**, 285.
10. N. C. Tice, C. A. Snyder, A. Z. Preston, M. B. Wieliczko, J. O. E. Young, and D. F. Hinson, *Transit. Met. Chem.*, 2012, **37**, 141.
11. C. A. Snyder, J. B. Maddox, J. O. E. Young, B. D. Garabato, J. W. Evans, L. A. Dopierala, S. A. Shah, Z. A. Claytor, A. C. Smith, N. C. Tice, and M. G. Mazzotta, *Transit. Met. Chem.*, 2013, **38**, 801.
12. J. E. O. Young, C. A. Snyder, N. C. Tice, S. L. Sloan, A. C. Smith, S. A. Shah, L. A. Dopierala, M. S. Crocker, Y. Kobayashi, and M. G. Mazzotta, *Synth. Commun.*, 2013, **43**, 2441.
13. S. Wild and N. Tice, *J. Mol. Model.*, 2021, **27**, 60.
14. A. Sabta, W. M. Eldehnab, T. Al-Warhic, O. J. Alotaibic, M. M. Elaasserd, H. Sulimane, and H. A. Abdel-Azizf, *J. Enzyme Inhib. Med. Chem.*, 2020, **35**, 1616.
15. C. Le Manach, D. G. Cabrera, F. Douelle, A. T. Nchinda, Y. Younis, D. Taylor, L. Wiesner, K. L. White, E. Ryan, C. March, S. Duffy, V. W. Avery, D. Waterson, M. J. Witty, S. Wittlin, S. A. Charman, L. J. Street, and K. Chibale, *J. Med. Chem.*, 2014, **57**, 2789.
16. A. Feraldi-Xypolia, D. G. Pardo, and J. Cossy, *Eur. J. Org. Chem.*, 2018, 3541.
17. R. H. Bradbury, N. J. Hales, A. A. Rabow, G. E. Walker, D. G. Acton, D. M. Andrews, P. Ballard, N. A. N. Brooks, N. Colclough, A. Girdwood, U. J. Hancox, O. Jones, D. Jude, S. A. Loddick, and A. A. Mortlock, *Bioorg. Med. Chem. Lett.*, 2011, **21**, 5442.
18. M. Krier, J. X. de Araūjo-Jūnior, M. Schmitt, J. Duranton, H. Justiano-Basaran, C. Lugnier, J.-J. Bourguignon, and D. Rognan, *J. Med. Chem.*, 2005, **48**, 3816.
19. D. Amariucai-Mantu, V. Mangalagiu, and I. I. Mangalagiu, *Molecules*, 2021, **26**, 3359.
20. A. Garrido, G. Vera, P. Delaye, and C. Enguehard-Gueiffier, *Eur. J. Med. Chem.*, 2021, **226**, 113867.
21. W. Linn and W. Sharkey, *J. Am. Chem. Soc.*, 1957, **79**, 4970.
22. C. Snyder, N. Tice, P. Sriramula, J. Neathery, J. Mobley, C. Phillips, A. Preston, J. Strain, E. Vanover,

M. Starling, N. Sahi, and K. Bunnell, *Synth. Commun.*, 2011, **41**, 1357.

23. N. Tice, E. Collins, D. Smith, C. Snyder, B. Yan, and E. Stevens, *J. Heterocycl. Chem.*, 2017, **54**, 3235.
24. C. Snyder, N. Tice, J. Maddox, S. Parkin, A. Daniel, and J. Thomas, *Heterocycles*, 2011, **83**, 1275.
25. N. C. Tice, S. Wild, C. Olmstead, E. D. Stevens, B. Yan, H. Brooks, and J. L. Jenkins, *Heterocycles*, 2019, **98**, 1707.
26. CCDC 2204847 contains the supplementary crystallographic data for this paper. These data can be obtained free of charge from The Cambridge Crystallographic Data Centre via www.ccdc.cam.ac.uk/data_request/cif.
27. Gaussian 16, Revision B.01, M. Frisch, G. Trucks, H. Schlegel, G. Scuseria, M. Robb, J. Cheeseman, G. Scalmani, V. Barone, G. Petersson, H. Nakatsuji, X. Li, M. Caricato, A. V. Marenich, J. Bloino, B. Janesko, R. Gomperts, B. Mennucci, H. Hratchian, J. Ortiz, A. Izmaylov, J. Sonnenberg, D. Williams-Young, F. Ding, F. Lipparini, F. Egidi, J. Goings, B. Peng, A. Petrone, T. Henderson, D. Ranasinghe, V. Zakrzewski, J. Gao, N. Rega, G. Zheng, W. Liang, M. Hada, M. Ehara, K. Toyota, R. Fukuda, J. Hasegawa, M. Ishida, T. Nakajima, Y. Honda, O. Kitao, H. Nakai, T. Vreven, K. Throssell, J. A. Montgomery, Jr., J. Peralta, F. Ogliaro, M. Bearpark, J. Heyd, K. Brothers, V. Kudin, T. Staroverov, R. Keith, J. Kobayashi, K. Normand, E. Raghavachari, A. Rendell, J. Burant, S. Iyengar, J. Tomasi, M. Cossi, J. Millam, M. Klene, C. Adamo, R. Cammi, J. Ochterski, R. Martin, K. Morokuma, O. Farkas, J. B. Foresman, and D. Fox, Gaussian, Inc., Wallingford CT, 2016.
28. GaussView, Version 6, R. Dennington, T. Keith, and J. Millam, Semichem Inc., Shawnee Mission, KS, 2016.
29. J. P. Perdew, K. Burke, and M. Ernzerhof, *Phys. Rev. Lett.*, 1996, **77**, 3865.
30. T. H. Dunning Jr., *J. Chem. Phys.*, 1989, **90**, 1007.
31. For more information on the Pearson correlation coefficient, see: S. Glen, Correlation Coefficient: Simple Definition, Formula, Easy Steps, Available from StatisticsHowTo.com: Elementary Statistics for the rest of us! https://www.statisticshowto.com/probability-and-statistics/correlation-coefficient-formula/
32. K. P. S. Hussan, K. A. A. Rahoof, M. Z. Medammal, S. Thayyil, and T. D. Babu, *Free Radic. Res.*, 2022, **1**, 53.
33. K. G. Sangeetha, K. K. Aravindakshan, and K. P. Safna Hussan, *J. Mol. Struct.*, 2017, **1150**, 135.
34. NBO Version 3.1, E. D. Glendening, A. E. Reed, J. E. Carpenter, and F. Weinhold.
35. H. Gökce, G. Alpaslan, and C. Alaşalvar, *J. Coord. Chem.*, 2019, **72**, 1075.
36. J. A. Agwupuye, P. A. Neji, H. Louis, J. O. Odey, T. O. Unimuke, E. A. Bisiong, and T. N. Ntui, *Heliyon*, 2021, **7**, e07544.

37. K. Sathesh Kumar, N. Haridharan, S. Ranjith, and A. Nataraj, *Chemical Physics Impact*, 2023, **6**, 100139.
38. G. M. Sheldrick, CELL_NOW 2008, Georg-August-Universität, Göttingen, Germany.
39. Bruker Apex3 v2019.11-0, SAINT V8.40A, 2019, Bruker AXS Inc.: Madison (WI), USA.
40. G. M. Sheldrick, *Acta Crystallogr., Sect. C*, 2015, **71**, 3.
41. G. M. Sheldrick, TWINABS 2012/1., 2012, Bruker, Madison, Wisconsin, USA.